Valeology: International Journal of Medical Anthropology and Bioethics
(ISSN 2995-4924) VOLUME 02 ISSUE 09, 2024

THE DFT ANALYSIS OF THE V2O5 COMPOUND'S STRUCTURAL, ELECTRONIC, AND OPTICAL PROPERTIES AND PHOTOCATALYTIC APPLICATIONS

Sattar H. Abed, Ali H. Reshak
Physics Department, College of Science, University of Basrah, Basrah, Iraq

Abstract:

The research discussed investigates the properties of a photocatalytic material containing metal oxides V2O5. X-ray diffraction analysis was used to improve the atomic arrangement in the material, and the generalized gradient approximation (GGA-PBE), was employed in electronic and optical calculations using the CASTEP code to analyze the structural configuration of the V2O5 compound. The optimized structure was used to calculate the electronic band structure and related properties using (GGA-PBE). It was determined that the bandgap of the material is a direct gap (Eg2.20eV)(GGA-PBE), which closely agrees with the experimental energy gap(2.3eV).Additionally, the study indicated that the O2p (valence band) and V4d (conduction band) states make a crucial role in governing the energy gap. The electronic charge density distribution was calculated to explore the chemical bonding properties, and the optical properties showed an increase in absorbance in the visible light region with an increase in particle concentration. Based on these characteristics, V2O5 compound is considered a suitable material for photocatalytic applications.

Keywords: V2O5, Band Structure, GGA-PBE, DFT, photocatalytic.

Introduction

1. Introduction

Environmental purification is a significant and globally significant scientific field [1-6]. Environmental concerns have increased due to industrial dangers, with manufacturing waste and harmful energy sources causing around 20% of water contamination [4-9]. Liquid waste, containing numerous organic, chemical, and biological contaminants, poses a significant threat to both individuals and the environment. [9,10–16]. Various methods have been used to convert hazardous waste into usable form, but most are expensive and require significant energy. Semiconductor photocatalysis treatment is an environmentally friendly method for removing harmful pollutants from wastewater[17-21]. V_2O_5 is a promising material for n-type semiconductors due to its adjustable bandgap within the visible-light range, specifically between 1.8 and 2.7 eV [17,20-26]. The material's exceptional chemical stability and non-toxicity make it an ideal choice for photocatalysis for breaking down organic effluent. [24-27]. The composition of nanoparticles significantly influences their ability to catalase chemical reactions through light, according to recent research. [28–35]. Density functional theory (DFT) can explain processes like analyzing pollutants and producing clean energy, such as hydrogen production and biological pollutants, using experimentally prepared compounds [33,36-39]. The structural configuration of the V_2O_5 compound was analyzed using the generalized gradient approximation (GGA-PBE) in electronic and optical calculations using the CASTEP code[40-43].The optimized structure was utilized to calculate the electronic band structure and properties using (GGA-PBE), revealing a direct energy gap of 2.20eV, which closely matches the experimental gap value of 2.20 eV [32,41,45]. The study revealed that the O_2p (valence band) and V4d (conduction band) states significantly influence the energy gap[41,43,46]. The study calculated the electronic charge density distribution to investigate chemical bonding properties, revealing an increase in absorbance in the visible light region with increased particle concentration.

2. Computational methodology

The study utilized the CASTEP algorithm to analyze the electrical and structural properties of V_2O_5, a 40-atom material, using Density Functional Theory (DFT) to understand the photocatalytic efficiency of V_2O_5 nanoparticles, resulting in highly accurate results. This systematic approach in computer-based problem solving and analysis is crucial. [41]. The calculations were based on crystallographic information from a single X-ray diffraction, using the generalized gradient approximation with the Perdew-Burke-Ernzerhof parameterization [42,43]. The interactions between ionic cores and valence electrons were characterized using a norm-conserving pseudopotential [44]. The Brillouin zone was sampled using a Monkhorst-Pack k-point mesh and a plane wave basis with an energy cut-off of 430 eV. Convergence conditions for atomic force and mass were established with thresholds of 0.05 eV.

3. Results and discussion

3.1 Structural properties

Vanadium pentoxide (V_2O_5) is found in the orthorhombic phase of the crystal lattice in the Pnma (No. 62) space group. The lattice constants were experimentally determined and optimized using the generalized gradient approximation (GGA) PBE method Table(1)[48].The results for lattice constants show a close agreement between theoretical and optimized results, indicating high accuracy in atomic arrangement, internal angles, and crystal packing, as shown in Figures(1) and Table(2)[49].

Table (1). It represents data on the structural properties of the compound V_2O_5.

Lattice type P Space group name P n m a Space group number 62					
Lattice parameters					
a(Å)	b(Å)	c (Å)	α	β	γ
9.68870	11.57820	3.61670	90°	90°	90°
Unit-cell volume = 405.713103 Å³					

Figure (1): The Crystal structure and arrangement of atoms of the compound V2O5.

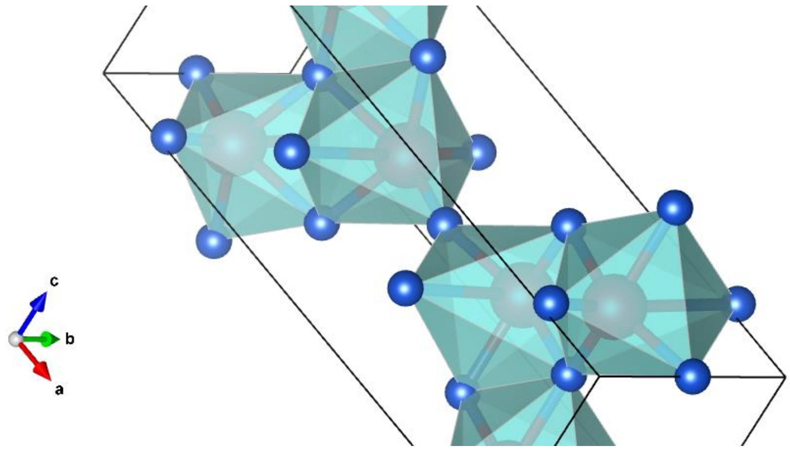

Table (2). Represents the theoretical (COD), geometrically optimized lattice constants of a compound V_2O_5.

Compound	a(Å)	b (Å)	c (Å)	V(Å³)
optimized Lattice parameters	9.688718	11.578192	3.616677	405.711004
Reciprocal Lattice	0.648505334	0.542674133	1.737281296	0.61396316
Lattice parameters COD (9012220)	9.68870	11.57820	3.616670	405.713103

Figure (3): Geometric optimization and energy of crystal lattice constants.

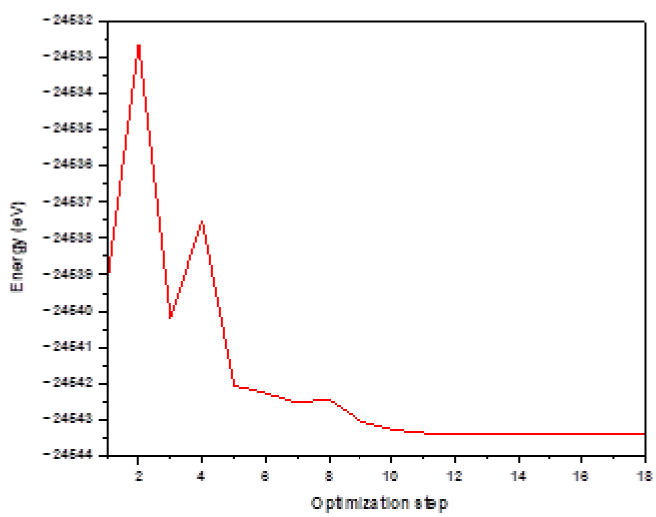

3.2. Electronic properties

3.2.1 Band Structure Electronic

To study the electronic behavior of V_2O_5, We calculated the electronic band structures and total and partial densities of states using several potentials, including GGA-PEB. For all calculations, the Fermi energy level E_f is defined as 0 eV. This energy level corresponds to both the highest energy level in the valence band (VB) and the lowest energy level in the conduction band (CB)[48]. The band structure is a critical characteristic in solid-state physics because it directly or indirectly influences all physical properties of materials through the band gap[49,50]. The results for V_2O_5

show that the valence band maximum (VB_M) and conduction band minimum (CB_M) occupy a single position, the K-point, represented by the coordinates Y, S, and K.Therefore, the semiconducting compound exhibits both direct and indirect energy gaps. This result aligns with the theoretical results (Fig. 3 a, b), which show a false indirect energy gap of 2.20 eV and a direct gap of approximately 2.21 eV. Table 3 displays other Present work and theoretical works related to the compound's energy. The figure illustrates the metallic behavior of the metal oxide material.

Table (3): The energy gap is the Present work and theoretical V2O5 results.

Compound	Present work	The researchers [49,5]	
V_2O_5	2.280 eV	2.264eV	Theoretical
	2.20 eV	2.21eV	approximately

Figure (4) represents the electronic band structure of a compound V_2O_5.

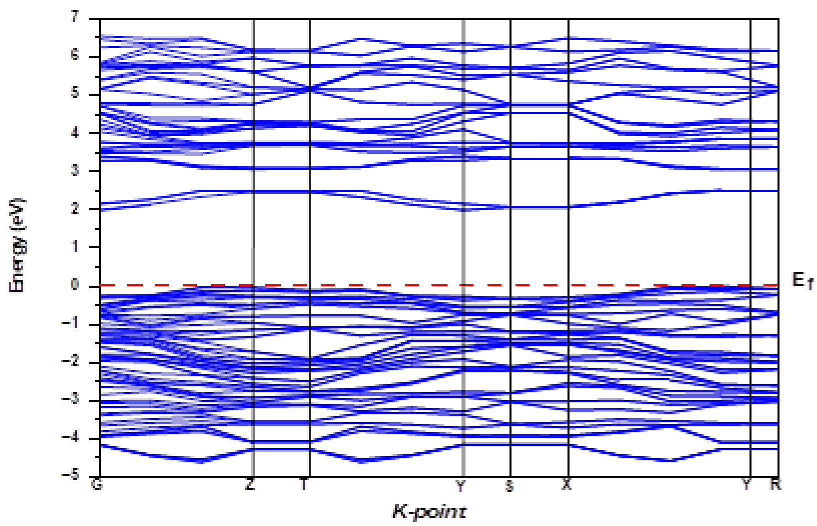

3.2.2. Total Density of States (TDOS) and Partial Density of States (PDOS).

The band structures of V_2O_5 compounds, with varying cross-linking potential levels, closely resemble real results due to spin-orbital interaction. Understanding the density of states helps comprehend electronic band structures and their impact on electron energy levels[51]. Figure (5a) displays the overall density of states (TDOS), whereas Figure (5b) illustrates the partial density. The Figure (5a) shows how V_2O_5's total density of states (TDOS) changes when the exchange link potential changes. Semiconductors possess distinctive characteristics due to the narrow energy gap between the valence band (VB) and the conduction band (CB) at the Fermi level. This shows that the potential densities of GGA and GGA-PEB are nearly identical, with only slight variations[49,52]. This highlights the potential of GGA-PEB in highly interconnected materials. that the partial density of state energy for the Fermi energy level, which is 2.64 to 2.20 eV. Figure (5b) demonstrates that the atomic states of d_V, s_V, and p_O have the greatest influence on the valence band (VB) of the state with an energy range of (1.18–6.77) eV. For PDOS practitioners, both of them are unappealing. The valence band peaks d_V, s_V, and p_O are located at an energy level of -5.31 eV. The primary contribution arises from T(V_O), which reaches its maximum at (-2_-2.46)eV in the lower valence band. Figure 13 shows that the conduction band, with a value of 3.31eV, contains the energy levels with the maximum energy, denoted as T (O_V). The states V_s, V_d, and O_s are located at distinct energy levels within the valence band, as depicted in the figure below. V_2O_5 is semiconducting because none of these states are above the Fermi energy level. These beneficial features simplify the management of exchange and correlation in highly correlated photocatalytic systems, resulting in improved outcomes consistent with experimental observations[55].

Figure 5: (a) represents the total density of states (TDOS). (b) represents the Partial density of states (PDOS).

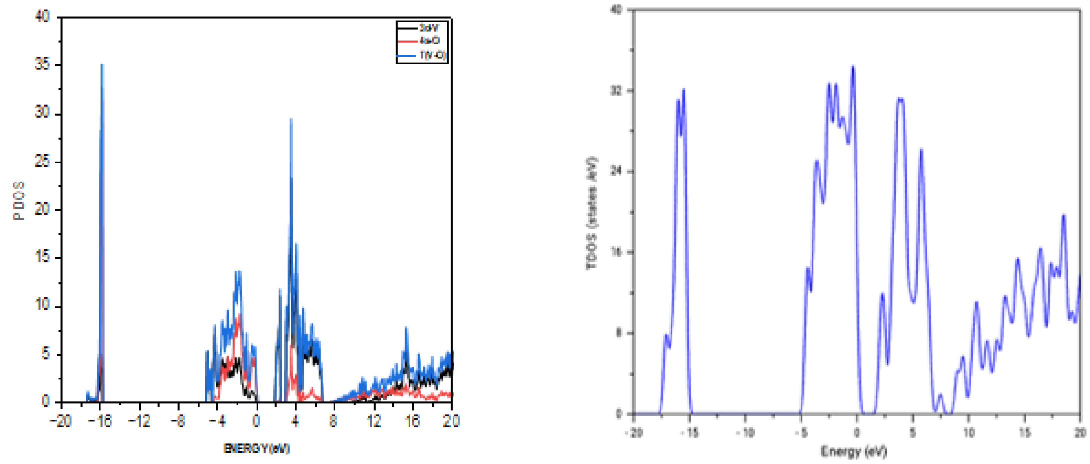

3.3. Optical properties results

A study was conducted on the optical properties of V_2O_5 under different conditions as a direct bandgap material with medium bandgap energy. The calculated bandgap energy for V_2O_5 is 2.20 eV for materials that are active in the visible light region. These materials, due to the bandgap, have many applications in optical detectors and photo-stimulated devices [50,49]. To understand the material's optical characteristics, it is necessary to know the energy loss function, efficiency, real and imaginary dielectric constants, refractive index, and oscillator strength. We computed the given parameters for the first time, as shown in figure (6). The chemical's polarizability is dependent on the inherent component of the dielectric function. The real portion of the dielectric function with an external photon energy of 0 eV is 5.89. A photon with an energy of 4.16eV from an external source can reach a maximum value of 9.26 when directed towards a target. As the external photon's frequency increases, its value declines with periodic fluctuations and ultimately hits zero at 6.52 eV. As the external energy increases, the refractive index's value begins to rise again. Once it reaches 20 eV, the refractive index becomes saturated. The computed outcomes for V_2O_5 are displayed in Figure (6). We often use the imaginary portion of the dielectric function to describe the absorption of light by a material. The high magnitudes of the imaginary component of the dielectric function indicate substantial light absorption[50-54]. The complex component of the dielectric function is seen in Figure (6). The data suggests that the V_2O_5 material begins absorbing energy at a threshold of 2.28 eV and continues to absorb more energy until it reaches a peak at 9.28 eV. However, within the energy range of 7.53 eV, the absorption steadily declines to a value of 0.978 at 10 eV. The peaks observed in the figure correspond to distinct transitions between the estimated conduction and valence bands[52-55].

Figure (6): shows the Real $\varepsilon_1(\omega)$ and Imaginary $\varepsilon_2(\omega)$ Dielectric functions.

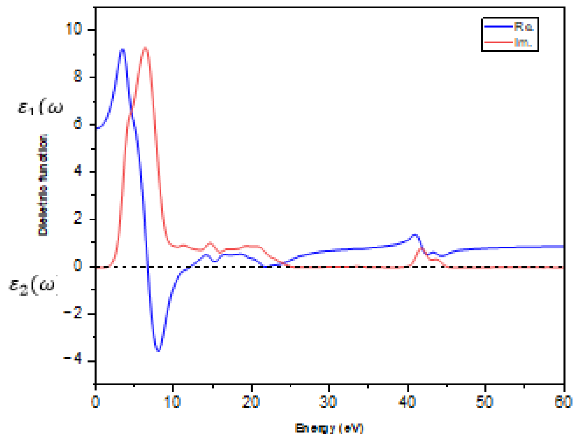

We determined the refractive index of V_2O_5 for the first time. Figure (15) displays the refractive index n (ω) of V_2O_5. The refractive index changes in response to incoming photon energy. When there are no external photons with an energy of 0 eV, the determine the refractive index of V_2O_5 to be 2.48. The value steadily diminishes as the intensity drops and reaches 0.46 when the incoming photon has an energy of 9.28 eV. The stimulation and relaxation processes, which include many internal energy levels in V_2O_5, cause a slight deviation in the refractive index. The provided Figure (7) displays the extinction coefficient k(ω), which reaches its highest value throughout the energy range of extinction between 2.81 eV and 9.16 eV. The coefficient ranges from 0 to 2.43. The numerous peaks in the curve are a result of the transitions that occur between the valence band and the conduction band. The compound's strong light absorption is responsible for its high extinction coefficient[54,55].

Figure (7): shows the refractive index n(ω) and extinction coefficient k(ω).

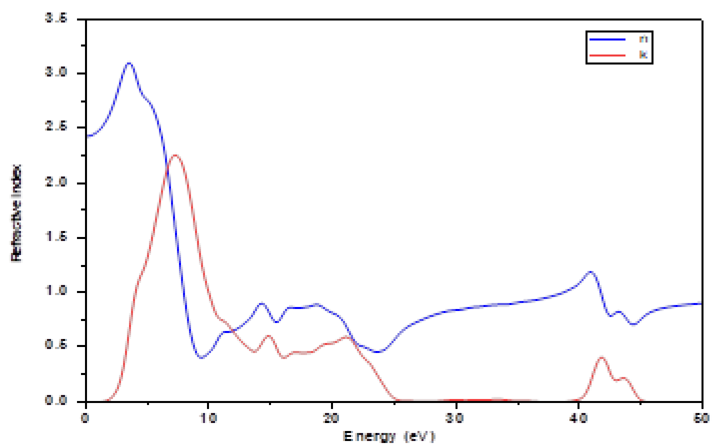

The reflectivity R(ω) of V_2O_5 was computed and is depicted in Figure(8). Reflectance unequivocally exposes the inherent characteristics of a material's surface[55]. The reflectance of V_2O_5 is approximately 0.79 in the absence of external photons (0 eV). The reflectance has a clear pattern of reaching its lowest point at 35 eV and its highest point at 9.28 eV, which may be attributed to plasmon resonance.

Figure (8): shows the calculated reflectivity spectra of V_2O_5.

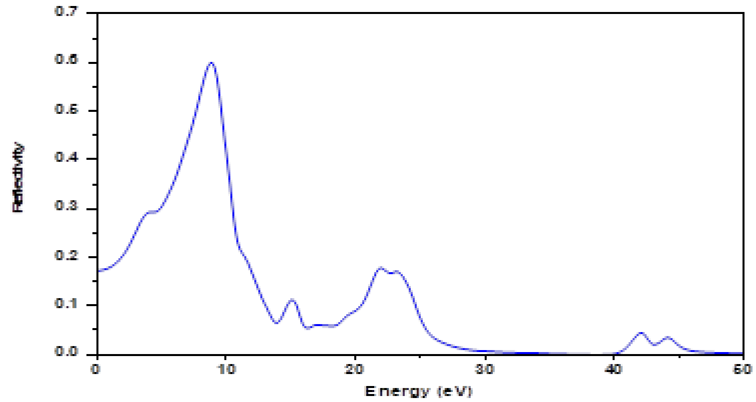

One may provide a clear understanding of several factors, such as transmission, reflection, and reflectance, by doing a spectral analysis of the Energy Loss Function (ELF) [52-55]. Researchers can investigate the characteristics of the targeted atom and the dispersed and absorbed photons using the energy loss function [45-56]. Figure (9) displays the computed electron loss function (ELF) for vanadium pentoxide (V_2O_5). We found dispersion and transparency in V_2O_5, without any photon scattering. We investigated inelastic scattering and found that the medium energy range had the highest energy loss. We discovered that the peak values occurred in the energy range of 24.31 eV. Using the sum rule, we determined the effective electron count associated with the optical transitions. The oscillator strength quantifies the intensity of transitions occurring between the valence and conduction bands. Because of an electronic band gap, a partial density of states, and an ELF (Electron Loss Function) analysis, these materials have electronic activity[55].

Figure (9): The energy loss function (ELF) for the compound V_2O_5.

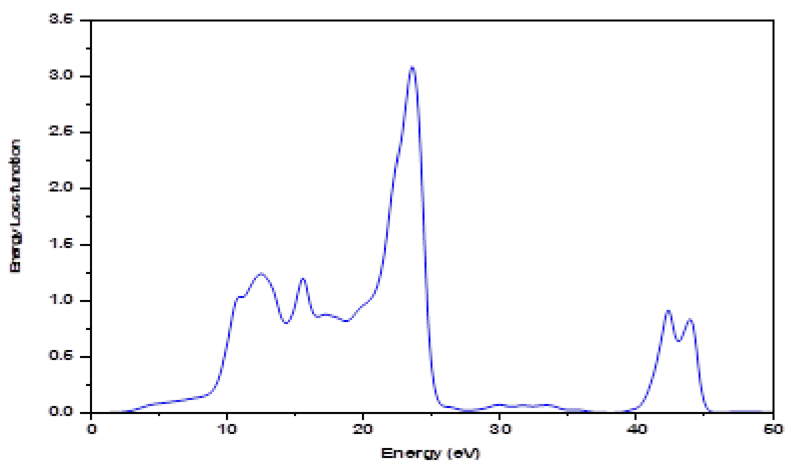

On the other hand, the conductivity of the V_2O_5 compound, which lies between the valence and conduction bands, is essential for electron transitions between the two bands and energy levels that are crucial in photocatalysis processes, solar cells, and electronic detectors[55]. Through Figure(10), the conductivity starts at (0 $\Omega^{-1}cm^{-1}$) with an energy of 2.18 eV and increases to 7.5 $\Omega^{-1}cm^{-1}$ at 7.29 eV, then gradually decreases to (0 $\Omega^{-1}cm^{-1}$) at an energy of 25.7 eV. Afterward, it starts growing again at 40 eV, indicating that it is optically active.

Figure (10): the conductivity to compound V_2O_5 by method (GGA-PEB).

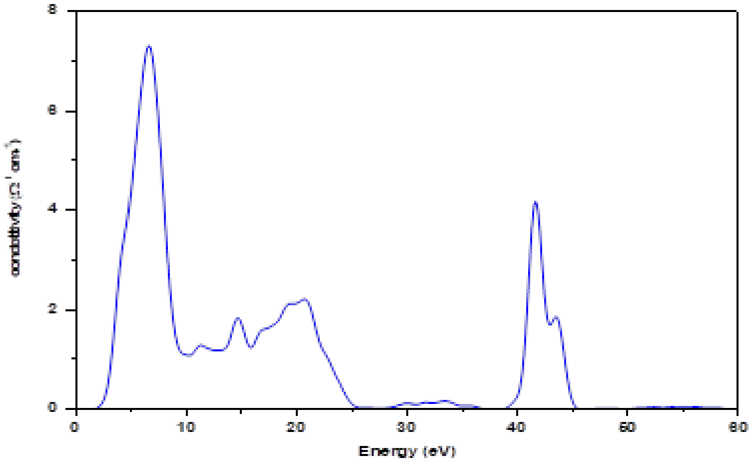

3.4. photodegradation

In order to get a deeper understanding of the experimentally reported results, a computational analysis based on density functional theory (DFT) was conducted. This work involved creating an orthorhombic supercell of V_2O_5. The supercell structure of V_2O_5, which has been improved, is seen in Figure (3). The mean bond distance between V and O in this study is 1.8554 Å, which closely corresponds to previously documented measurements. The efficacy of dye degradation in a nanoparticle can be assessed by utilizing a limited number of factors derived from DFT simulations. The topics of interest are[54-56]: (i) the band gap of V_2O_5, (ii) the electronic properties of V_2O_5, and (iii) the optical properties of V_2O_5. The developed V_2O_5 supercell has a visible area bandgap value of 2.20 eV in the present study. The PDOS spectrum (Fig. 5b) demonstrates the orbital impact of the V and O atoms. The figure clearly demonstrates that the presence of O_p orbitals has a significant impact on the valence band. However, the V_d orbitals on the conduction band side provide the majority of the energy levels. These orbitals facilitate the transmission of electric charge between the valence and conduction bands[55-57]. In addition, there are a lot of different energy states in both the valence and conduction bands. This is because vanadium (V) atoms have 3d orbitals and oxygen (O) atoms have 2p orbitals. The redox capability of V_2O_5 can be attributed to the band edge potentials, which have a pivotal role in oxidation and reduction reactions. The band edge potentials for the V_2O_5 nanostructure are determined using the following equations[43].

Figure (11): the photodegradation to compound V_2O_5 by method (GGA-PEB).

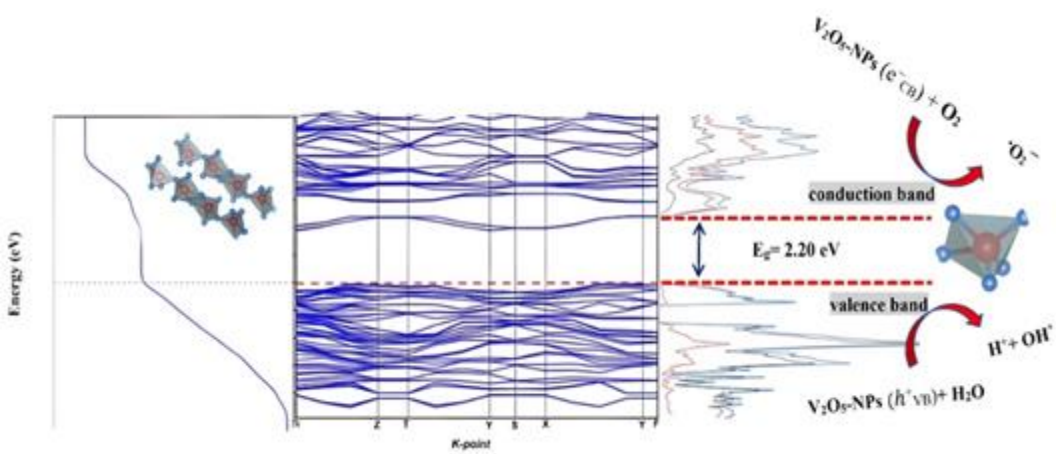

$$E_{vb} = \chi - E_e + \frac{1}{2}(E_g)\, E_{cb} = E_{vb} - E_g$$

Here, E_e represents the energy of an unbound electron on the hydrogen scale, E_g designates the calculated energy difference, and χ represents the electronegativity. The valence band and conduction band edge potentials have been determined to be 1.9575 eV and -0.2425 eV, respectively. The V_2O_5's calculated band edge potentials meet the requirements for a good photocatalytic material[55]. The valence band potential is higher than 1.9575 eV, and the conduction band edge is lower than -0.2425 eV. The relevant potentials mentioned are the standard normal hydrogen electrode (NHE) potentials used for scaling efficient photocatalytic materials [54-56].Charge-free carrier mobility is employed as a measure to assess the photocatalytic activity of V_2O_5. The increased mobility of the charge carriers results in a reduction in the rate of recombination, hence enhancing the rates of redox reactions. To quantify mobility, one can determine the effective mass (m^*) of the charge carriers. Based on the findings in the literature [58-60], it is necessary for the effective mass of charge carriers in a nano-photocatalytic material to be less than 0.5 me in all crystallographic orientations. The present investigation has established that the effective mass of charge carriers in V_2O_5 is 0.473 times the electron mass. This leads to a reduction in the diffusion coefficient, resulting in a drop in the rate of recombination. An in-depth understanding of the light absorption properties of the V_2O_5 nanostructure can be gained by examining its imaginary component of the frequency-dependent dielectric function. The dielectric function in this study was determined by calculating the in-plane $\varepsilon_1(\omega)$ and plane $\varepsilon_2(\omega)$ dielectric functions, as shown in Figure (14). When examining the actual portion of the spectrum, specifically the real dielectric function mode $\varepsilon_1(\omega)$, it becomes evident that there is no alteration in magnitude. This implies that the entirety of the radiation is traversing the structure. However, there is a notable reduction in the amplitude observed for the out-of-plane mode ($\varepsilon_1(\omega)$), indicating that the structure is unable to transmit radiation in these energy ranges. However, upon examining the imaginary component, it is clear that there is once again no absorption of the incident radiation in the in-plane mode[58-63]. However, we see a distinct peak in the visible region for the out-of-plane mode. According to the DFT calculations, it is evident that the V_2O_5 structure is a feasible choice for photocatalytic reactions that are powered by visible light[55].

The charge density charts of the valence band maximum (VB_M) and the conduction band minimum (CB_M) states projected on the (010) plane for both configurations are shown in Figure (12). The valence bond model (VBM) state of V_2O_5 arises from the notable V-O bond length, with the majority of the charge density focused on the oxygen ions. The CBM state is generated by the hybridization of d_V, s_V, and p_O. A band [62,64] separates, and the charge density map indicates enhanced orbital overlap between the V_ 3d and O_ 2p states. The separated group serves to restrict electric charge and has been proven to be responsible for the formation of large polarons, resulting in uneven alkali intercalation [65]. The charge density plot of the valence band maximum (VB_M) indicates that the O ion has the largest concentration of electron density. The distribution exhibits spherical symmetry, indicating the existence of ionic bonding. For systems that do not exhibit any spin polarization, the electronic structure can be correctly described using Density Functional Theory (DFT) at the Generalized Gradient Approximation (GGA) level. Further improvement can be attained by considering on-site Coulombic interactions, which encompass the lattice characteristics and electronic structure of different elements[59-64].

Figure (12): The charge density distribution of V_2O_5 in (010) crystallographic.

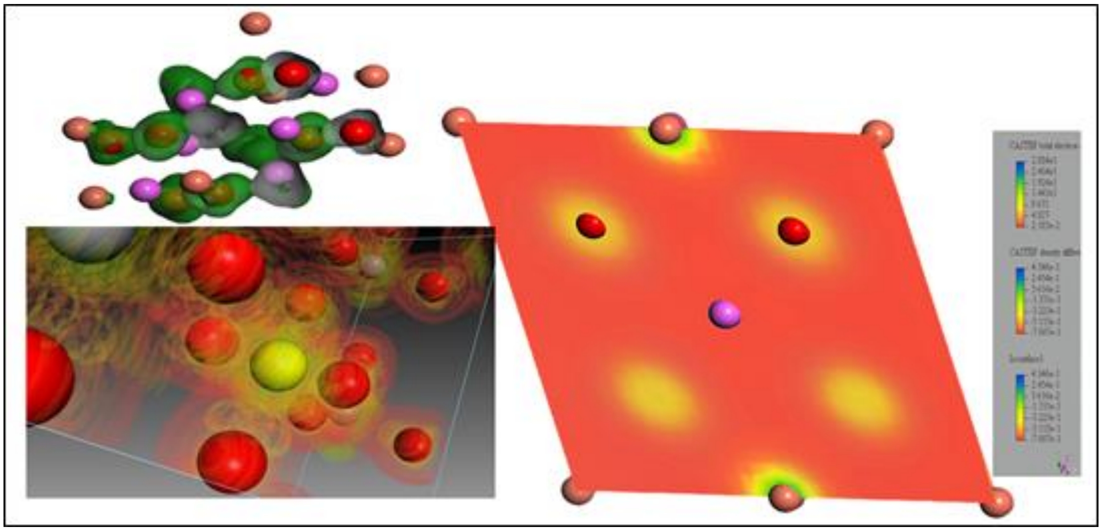

Recent research have employed (DFT) and (GGA) calculations to examine However, the band gap value grows as the value of Ue increases. This increase is attributed to the charge distribution in the V-O bond, specifically the splitting of the band. Many individuals often use a widely known value of Ueff = 3.0 eV for V_2O_5, as it results in a band gap that roughly corresponds to experimental observations[65,66].

4. Conclusions

The study investigated the use of V2O5 as active photocatalysts using the PBE-GGA method. It examined the optical, structural, photocatalytic, and transport properties of these metal oxide semiconductors. The effect of vanadium (V) and oxygen (O2) on these properties was also studied. The optical properties showed an absorption edge shift to $\lambda = 563.63$ nanometers, which aligns with the solar spectrum. The electronic structure and angular momentum characteristics confirmed electron charge distribution, revealing a clear map of electron charge transfer and chemical bonding. The charge density distribution showed a high concentration of charge density on oxygen ions in the valence band maximum (VBM) and an optimized orbital overlap between vanadium and oxygen in the conduction band minimum (CBM). This led to the formation of electron-hole recombination inhibitors (e_h) and limited electrical charge leakage in the alkaline interface. The bandgap value increased with the Ue value, and Ueff = 3.0 eV was preferred for organic material analysis.

ACKNOWLEDGEMENTS

The authors gratefully acknowledge support from department of Physics, College of Science, University of Basrah, Iraq .

Author Contributions: Sattar H. Abed wrote the main manuscript text and prepared all figures. Ali H. Reshak supervised the manuscript and edited the manuscript .

Ethical Approval: The study protocol was approved by local ethics committee.

References

1. J. Kaur, T. Pathak, A. Singh, and K. Kumar, "Application of Nano technology in the environment biotechnology," in Advances in Environmental Biotechnology, Springer, 2017, pp. 155-165
2. J. Zhang, B. Tian, L. Wang, M. Xing, and J. Lei, Photocatalysis: fundamentals, materials and applications, vol. 100. Springer, 2018.

3. M. Pelaez et al., "A review on the visible light active titanium dioxide photocatalysts for environmental applications," Appl. Catal. B Environ., vol.125, pp. 331-349, 2012, doi: 10.1016/j.apcatb.2012.05.036.

4. H-s, lee j, lee s, et al." Walnut-like ZnO-Zn_2TiO4 multicore shell submicron spheres with a thin carbon layer: fine synthesis; facile structural control and solar light photocatalytic application". Acta material; 2017, 122(287-97).

5. S. H. Abed and A. H. Reshak, "Illuminating the Power of V2O5 Nanoparticles: Efficient Photocatalytic Degradation of Organic Dyes under Visible Light," *J. Fluoresc.*, 2024, doi: 10.1007/s10895-024-03841-3.

6. n. N, z. L, f. J, et al. Self-assembled hierarchical direct z-scheme g-c3n4: zno microspheres enhanced photocatalytic co2 reduction performance. Applied surface science, 2018. 441;(12-22).

7. O. Legrini, E. Oliveros, and A. M. Braun, "Photochemical processes Iorwater treatment" Chem. Rev., vol. 93, no. 2, pp. 671-698, 1993.

8. N. Luis and J.-A. Wang, Advanced Catalytic Materials: Photocatalysis and Other Current Trends. BoD-Books on Demand, 2016.

9. C. Byrne, G. Subramanian, and S. C. Pillai, "Recent advances inphotocatalysis for environmental applications," J. Environ. Chem. Eng., vol.6, no. 3, pp. 3531-3555, 2018.

10. K. Sharma, A. S. Al-Kabbi, G. S. S. Saini, and S. K. Tripathi, "Indium doping induced modification of the structural, optical and electrical properties of nanocrystalline CdSe thin films," J. Alloys Compd., vol. 564, pp. 42–48, 2013, doi: 10.1016/j.jallcom.2013.02.037.

11. K. A. Mohammed et al., "Optical, morphological, electrical properties and white light photoresponse of CdSe nanoparticles," Adv. Mater. Process. Technol., vol. 8, no. sup4, pp. 2289–2298, 2022, doi: 10.1080/2374068X.2022.2037877.

12. T. Oyama, A. Aoshima, S. Horikoshi, H. Hidaka, J. Zhao, and N. Serpone,"Solar photocatalysis, photodegradation of a commercial detergent in aqueous TiO2 dispersions under sunlight irradiation," Sol. Energy, vol. 77,no. 5, pp. 525-532, 2004.

13. M. R. Khan, T. W. Chuan, A. Yousuf, M. N. K. Chowdhury, and C. K.Cheng, "Schottky barrier and surface plasmonic resonance phenomena towards the photocatalytic reaction: study of their mechanisms to enhance photocatalytic activity," Catal. Sci. Technol., vol. 5, no. 5, pp. 2522-2531,2015.

14. H. Kisch, "Semiconductor photocatalysis-mechanistic and synthetic aspects," Angew. Chemie Int. Ed., vol. 52, no. 3, pp. 812-847, 2013.

15. li j, wu n. Semiconductor-based photocatalysts and photoelectrochemical cells for solar fuel generation: a review. Catalysis science & technology, 2015, 5(3): 1360-84.

16. S. Rehman, R. Ullah, A. Butt, and N. D. Gohar, "Strategies of making $TiO_2$and ZnO visible light active," J. Hazard. Mater., vol. 170, no. 2-3, pp. 560569, 2009.

17. T. An et al., "Structural and photocatalytic hydrothermally treated mesa porous TiO2," Appl. Catal. A Gen., vol. 350,no. 2, pp. 237-243, 2008.

18. P. Gharavi s m, xie l, webster r f, et al. Interfacial origins of visible-light photocatalytic activity in ZnS–gap multilayers. Acta materialia, 181139-47,2019.

19. k. Edalati, uehiro r, takechi s, et al. Enhanced photocatalytic hydrogen production on gan–ZnO oxynitride by introduction of strain-induced nitrogen vacancy complexes. Acta materialia, 2020, 185(149-56).
20. F. Y, cheng h, h., et al. Chlorophyll sensitized bi VO_4 as photo anode for solar water splitting and CO_2 conversion. Chinese chemical letters; 2017. 28(12); 2254-8
21. mònica, calatayud and et al. A periodic model for the V_2O_5–TiO2 (anatase) catalyst. Stability of dimeric species. 2003.
22. M. calatayud, minot c. Reactivity of the oxygen sites in the V2O5–TiO2 (anatase) catalyst. The journal of physical chemistry b, 2004, 108(40): 15679-85.
23. B. Bhuyan, B. Paul, S.S. Dhar, Cetyltrimethy lammonium bromide promoted size tuning synthesis of rod like V_2O_5 nanoparticles and their catalytic studies in oxidative esterification of aldehydes; Nanosci; Nanotechnol. Lett. 8 (2016).
24. S. N. Ahmed and W. Haider, "Heterogeneous photocatalysis and itspotential applications in water and wastewater treatment: a review,"Nanotechnology, vol. 29, no. 34, p. 342001, 2018.
25. A. Mohamed, R. El-Sayed, T. A. Osman, M. S. Toprak, M. Muhammed, andA. Uheida, "Composite Nano fibers for highly efficient photocatalytic degradation of organic dyes from contaminated water," Environ. Res., vol.145, pp. 18-25, 2016.
26. D. A. Friesen, L. Morello, J. V Headley, and C. H. Langford, "Factorsinfluencing relative efficiency in photo-oxidations of organic molecules byCs3PW12040 and TiO2 colloidal photocatalysts," J. Photochem. Photobiol.A Chem., vol. 133, no. 3, pp. 213-220, 2000.
27. R. Vinu and G. Madras, "Photocatalytic Degradation of Water Pollutants Using Nano-TiO 2," in Energy efficiency and renewable energy through nanotechnology, Springer, 2011, pp. 625-677.
28. S. Linic, P. Christopher, and D. B. Ingram, "Plasmonic-metal nanostructures for efficient conversion of solar to chemical energy," Nat. Mater., vol. 10.no. 12, pp. 911-921, 2011.
29. Y. Cai, X. Li, Y. Zhang, X. Wei, K. Wang, and J. Chen, "Highly Efficient Dehydrogenation of Formic Acid over a Palladium-Nanoparticle-Based Mott-Schottky Photocatalyst," Angew. Chemie, vol. 125, no. 45, pp. 1203812041, 2013.
30. B. Rusinque, "Hydrogen Production by Photocatalytic Water SplittingUnder Near-UV and Visible Light Using Doped Pt and Pd TiO2," 2018.
31. J. Arana et al., "Photocatalytic degradation of formaldehyde containing wastewater from veterinarian laboratories," Chemosphere, vol. 55, no. 6, pp.893-904, 2004.
32. D. Jing et al., "Efficient solar hydrogen production by photocatalytic water Splitting: from fundamental study to pilot demonstration, Int. Hydrogen Energy, vol. 35, no. 13, pp. 7087-7097, 2010.
33. A. H. Reshak and S. Auluck, "Photocatalytic water-splitting solar-to-hydrogen energy conversion: Novel LiMoO3(IO3) molybdenyl iodate based on WO3-type sheets," J. Catal., vol. 351, pp. 1–9, 2017.
34. A. H. Reshak, "Photocatalytic water splitting solar-to-hydrogen energy conversion: Perovskite-type hydride XBeH3 (X = Li or Na) as active photocatalysts," J. Catal., vol. 351, pp. 119–129, 2017.
35. A. H. Reshak, "Sulfide oxide XZnSO (X = Ca or Sr) as novel active photocatalytic water splitting solar-to-hydrogen energy conversion," Appl. Catal. B Environ., vol. 225, no. December 2017, pp. 273–283, 2018.

36. A. H. Reshak, “Novel photocatalytic water splitting solar-to-hydrogen energy conversion: CdLa2S4 and CdLa2Se4 ternary semiconductor compounds,” Phys. Chem. Chem. Phys., vol. 20, no. 13, pp. 8848–8858, 2018.
37. H.J. Monkhorst, J.D. Pack, Special points for Brillouin-Zone integrations. Phys. Rev. B 13, 5188 (1976).
38. M. J. Al-anber, A. M. Ali, N. S. Al-Mailky, and A. H. Al-Mowali, “Theoretical DFT Study the Opto-electronic Properties of Poly(3,4-Ethylenedioxythiophene),” *Sci. World*, vol. 11, no. 11, pp. 66–69, 2013, doi: 10.3126/sw.v11i11.8555.
39. T. Jayaraman, S. Arumugam Raja, A. Priya, M. Jagannathan, M. Ashokkumar, "New J. Chem.," 339, 1367,(2015).
40. Chandrappa GT, Steunou N, Cassaignon S, Bauvais C, Livage J. 2003 Hydrothermal synthesis of vanadium oxide nanotubes from V2O5 gels. Catal. Today 78, 85–89.
41. F. Bahrani, R. Hameed, S. Resan, and M. Al-Anber, “Impact of Torsion Angles to Tune Efficient Dye-Sensitized Solar Cell/Donor-π-Acceptor Model Containing Triphenylamine: DFT/TD-DFT Study,” *Acta Phys. Pol. A*, vol. 141, no. 6, pp. 561–568, 2022, doi: 10.12693/APhysPolA.141.561.
42. Zhang X, Teng SY, Loy ACM, How BS, Leong WD, Tao X. 2020 Transition metal dichalcogenides for the application of pollution reduction: a review. Nanomaterials 10, 6.
43. Zhao J, Bremner SP, Ho-baillie A. 2018 Assessment of 2D materials and transition metal oxides as carrier selective contacts for silicon solar cells.
44. Raveesha R et al. 2022 Synthesis and characterization of novel thiazole derivatives as potential anticancer agents: molecular docking and DFT studies. Comput. Toxicol. 21, 100202.
45. Pramodh B et al. 2021 Synthesis, spectral characterization, crystal structure and theoretical investigation of (E)-3-(4-bromothiophen-2-yl)- 1-(5-bromothiophen-2-yl)prop-2-en-1-one. Chem. Data Collect. 31, 100587.
46. Fakharuddin A et al. 2021 Robust inorganic hole transport materials for organic and perovskite solar cells: insights into materials electronic properties and device performance. Sol. RRL 5,1–44.
47. Hossain, M. S., Zakaria, C. M., & Kudrat-E-Zahan, M. (2018). Metal complexes as potential antimicrobial agent: a review. American Journal of Heterocyclic Chemistry, 4(1), 1.
48. Galy, J., Darriet, J., Casalot, A., & Goodenough, J. B. (1970). Structure of the MxV2O5-β and MxV2− yTyO5-β phases. Journal of Solid State Chemistry, 1(3-4), 339-348.
49. Eyert, V., & Höck, K. H. (1998). Electronic structure of V 2 O 5: role of octahedral deformations. Physical Review B, 57(20), 12727.
50. M. Hadjab, S. Berrah, H. Abid, M. I. Ziane, H. Bennacer, and A. H. Reshak. First-principles investigation of the optical properties for Rock Salt mixed metal oxide MgxZn1−xO. Materials Chemistry and Physics, 182–189 (2016).
51. S. Berrah, A. Boukortt, H. Abid. Optical properties of the cubic alloy (In,Ga)N. Physica E: Low-Dimensional Systems and Nanostructures, Physica 41(4), 701–704(2009).
52. M. Fox. Optical Properties of Solids. Oxford University Press. American Journal of Physics **70**, 1269 (2002).

53. M. Dressel, and G. Gruner .Electrodynamics of Solids Optical Properties of Electrons in Matter. Cambridge University Press (2002)

54. C. Ambrosch-Draxl, J. O. Sofo. Linear optical properties of solids within the full-potential linearized augmented plane wave method. Computer Physics Communications 175. 1–14 (2006).

55. F. Chiker, Z. Kebbab, R. Miloua, and N. Benramdane. Birefringence of optically uni-axial ternary semiconductors. Solid State Communications, 151(21), 1568–1573 (2011).

56. M. Hadjab, S. Berrah, H. Abid, M. I. Ziane, H. Bennacer, and B. G. Yalcin. Full-potential calculations of structural and optoelectronic properties of cubic indium gallium arsenide semiconductor alloys. Optik 127(20), 9280– 9294 (2016).

57. B. Amin, R. Khenata, A. Bouhemadou, I. Ahmad, and M. Maqbool. Opto-electronic response of spinels MgAl2O4 and MgGa2O4 through modified Becke-Johnson exchange potential. Physica B: Condensed Matter, 407(13), 2588–2592 (2012).

58. Hossain, M. S., Zakaria, C. M., & Kudrat-E-Zahan, M. (2018). Metal complexes as potential antimicrobial agent: a review. American Journal of Heterocyclic Chemistry, 4(1), 1.

59. Galy, J., Darriet, J., Casalot, A., & Goodenough, J. B. (1970). Structure of the MxV2O5-β and MxV2− yTyO5-β phases. Journal of Solid State Chemistry, 1(3-4), 339-348.

60. Eyert, V., & Höck, K. H. (1998). Electronic structure of V 2 O 5: role of octahedral deformations. Physical Review B, 57(20), 12727.

61. Ranea, V. A., & Quiña, P. L. D. (2016). The structure of the bulk and the (001) surface of V2O5. A DFT+ U study. Materials Research Express, 3(8), 085005.

62. Regan, J. L., Schumacher, D., Staudte, S., Steffen, A., Haybaeck, J., Keilholz, U., ... & Lange, M. (2017). Non-canonical hedgehog signaling is a positive regulator of the WNT pathway and is required for the survival of colon cancer stem cells. Cell reports, 21(10), 2813-2828.

63. Tolhurst, T. M., Braun, C., Schnick, W., & Moewes, A. (2021). Comprehensive band gap and electronic structure investigations of the prominent phosphors M2Si5N8: Eu2+ (M= Ca, Sr, Ba) determined using soft X-ray spectroscopy and density functional theory. The Journal of Physical Chemistry C, 125(46), 25799-25806.